One-Dimensional Minigaps in Inversion Layer Subbands on High Index Surfaces of InSb

T. Evelbauer*, A. Wixforth, and J.P. Kotthaus
Institut für Angewandte Physik, Universität Hamburg,
Federal Republic of Germany

Dedicated to K. Dransfeld on the occasion of his 60th birthday

In metal-oxide-semiconductor structures prepared on high index surfaces of *p*-InSb one-dimensional minigaps are observed in the quasi-two-dimensional subband structure of the inversion layer electrons at low temperatures. From anisotropic structure in the inversion channel conductance energetical position and size of the minigap are deduced and studied in dependence on surface orientation. The measured energetical position of the minigap is well described by two models, the valley projection model by Sham et al. and the staircase interface model by Volkov et al. In the magnetoconductance the Shubnikov-de Haas oscillations are found to contain several periods, reflecting the possible electron orbits of a two-dimensional electron gas with a one-dimensional minigap in a magnetic field applied normal to the two-dimensional plane. The size of the minigap determined from magnetic breakdown is found to be comparable to the one deduced from the anisotropic structure in the zero-field conductance.

I. Introduction

One-dimensional (1D) minigaps in the subband structure of two-dimensional electron systems (2DES) on semiconductors were first discovered by Cole et al. [1] in metal-oxide-semiconductor field effect transistors (MOSFETs) fabricated on Si-surfaces with high Miller indices vicinal to Si(100). At liquid helium temperatures they observed anisotropic structure in the conductance versus gate voltage curves of the electron inversion layer as well as non-periodic Shubnikov-de Haas (SdH) oscillations in the magnetoconductance. They related these observations to the appearance of 1D minigaps in the originally 2D subband structure [2] caused by the effects of a periodic 1D superlattice potential on the 2DES as shown in Fig. 1. With increasing gate voltage or, equivalently, increasing Fermi energy E_F in the 2DES, structure appears in the inversion layer conductance when the Fermi energy passes through a minigap ΔE. From the gate voltage at which the conductance structure occurs Cole et al. could determine the energetical position and, via the known dispersion $E(k_x)$ of the 2DES in the absence of the superlattice potential (see Fig. 1a), the extension G of the first minizone. In a simple superlattice model as sketched in Fig. 1, one expects anomalies in the 2D density of states $D(E)$ and hence in the conductance at energies around the center of the nth minigap ($n=1,2,\ldots$) given by:

$$\mathbf{E} = [\hbar^2/(2\mathbf{m}^*)](\mathbf{nG}/2)^2, \qquad (1)$$

where m^* is the effective band structure mass. Using such a model Cole et al. determined the period of the superlattice potential as $L=2\pi/G$ but were unable to identify the mechanism that causes this period.

A first model that could quantitatively explain the position of the observed minigaps in energy-

---

* Present address: VALVO RHW der Philips GmbH, Stresemannallee 101, D-2000 Hamburg 54, FRG

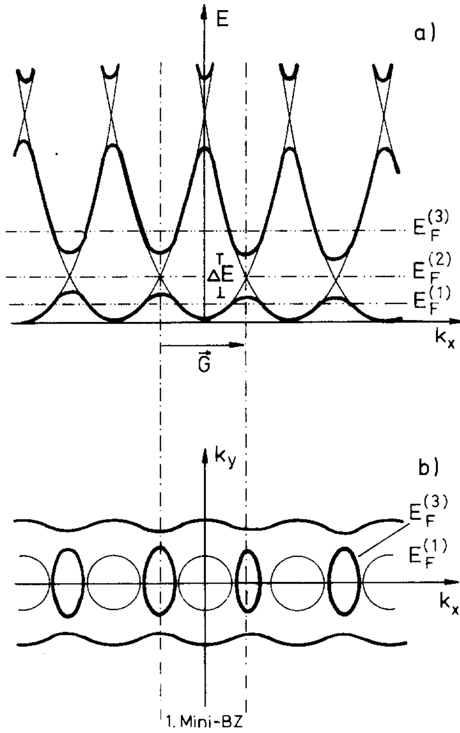

Fig. 1a and b. Schematic representation of one-dimensional minigaps in the subband structure of a single-valley two-dimensional electron system caused by a periodic superlattice potential with reciprocal lattice vector $\vec{G}$ parallel to the x-direction. **a** Energy-wavevector $E(k_x)$ relation in an extended mini-zone scheme for zero (thin line) and finite strength (heavy line) of the superlattice potential. Three characteristic positions of the Fermi energy E_F are indicated: $E_F^{(1)}$ in the lowest miniband, $E_F^{(2)}$ in the center of the lowest minigap, and $E_F^{(3)}$ in the 2nd miniband. **b** Fermi contours in the k_x-k_y plane for $E_F=E_F^{(1)}$ (thin line) and $E_F=E_F^{(3)}$ (heavy line). In the latter case lense-like and open orbits are possible

wavevector space was proposed by Sham et al. [3]. In this so-called valley projection model the Si $-SiO_2$ interface is assumed to be a plane with an infinite potential barrier for the inversion layer electrons. The constant energy contours in the 2DES are derived by projecting the bulk constant energy contours onto the interface plane. For a single valley semiconductor such as InSb this is illustrated for a high symmetry (low index) surface in Fig. 2a and for a high index surface, with its surface normal (z-direction) tilted by an angle θ with respect to the surface normal of the nearest high symmetry plane, in Fig. 2b. On a low index, high symmetry surface one thus obtains complete degeneracy of equivalent constant energy contours derived from different, adjacent Brillouin-zones and, for the case of a many valley semiconductor such as Si [3], from different but equivalent valleys. On a high index surface, however, this degeneracy only exists at discrete points in the k_x-k_y plane (see Fig. 2b). Along the k_x-direction these degeneracy points are periodic with a mini-zone period

$$\mathbf{G}=2\pi/\mathbf{L}=\mathbf{Q}\cdot\sin\theta \tag{2}$$

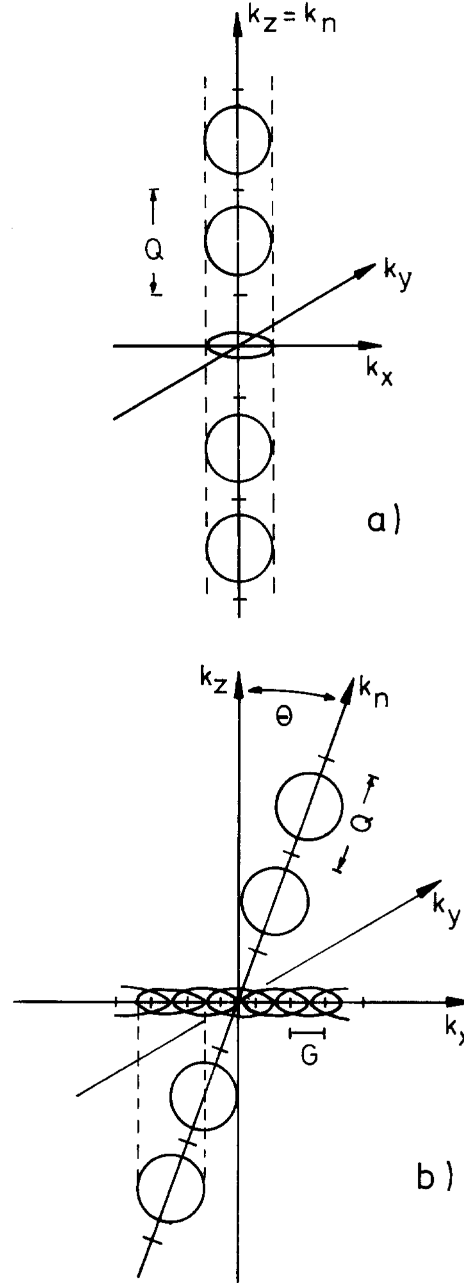

Fig. 2a and b. Valley projection model sketched for a single-valley semiconductor: **a** For a high symmetry surface the projection of bulk constant energy surfaces in adjacent Brillouin zones onto the respective surface yields fully degenerate energy contours. Here Q is the extension of the first Brillouin zone for the direction normal to the high symmetry surface (n-direction). **b** For a high Miller index surface with its normal (z-direction) tilted in the $x-z$ plane by an angle θ from the one of the high symmetry surface (n-direction). Here mini-zones of extension $G=Q\cdot\sin\theta$ are formed along the k_x-direction by projection of bulk constant energy contours in adjacent Brillouin-zones onto the high index surface

where Q is the length of the shortest reciprocal lattice vector along the direction normal to the next high symmetry plane. In the narrow inversion channel these degeneracies may be lifted by the effect of the interface boundary conditions thus giving rise to 1D minigaps. Two alternative models are used to describe such valley splittings first observed in electron inversion layers on Si(100) [4]: The so-called electric break through mechanism proposed by Ohkawa and Uemura [5] and a surface scattering model developed by Sham and Nakayama [6]. As has been pointed out by Ando [7, 8], both models are, however, essentially equivalent.

The valley projection model has been very successful to predict energetical positions of minigaps in electron inversion layers on surfaces vicinal to Si(100). Not only could it explain the energetical position of the lowest minigap observed by Cole et al. [1] as being caused by inter-valley interaction between non-equivalent valleys in adjacent Brillouin-zones. It also predicted minigaps created by intra-valley interaction such as shown in Fig. 1 which were subsequently observed in electron inversion layers on surfaces vicinal to Si(100) [9] and hole inversion layers on surfaces vicinal to Si(111) [10]. The valley projection model also has been rather successful to semi-quantitatively describe the experimental results observed in infrared optical studies of the interminiband absorption on Si surfaces [3, 11, 12].

There exists another model, the so-called staircase model, which can also explain all of the general features that are observed in the studies of 1D minigaps in MOS-structures on Si. This model, originally put forward by Volkov et al. [13, 14], is connected more directly with the real atomic properties of the semiconductor-oxide interface. It explains minigaps observed on high index surfaces as being caused by a periodical 1D staircase-like interface structure with steps of heights d and periodicity $L = d/\sin\theta$, as sketched in Fig. 3. Comparison with the valley projection model (Eq. (2) and Fig. 2) shows that these two models predict identical energetical positions of minigaps if the step heights $d = 2\pi/Q$. This relation and the fact that the valley projection model has correctly predicted all observed energetical positions of minigaps on surfaces of Si may be utilized to infer on the step heights d that may be expected for diamond or zincblende type crystals with an fcc Bravais lattice. For surfaces vicinal to (100) where $Q_{100} = 4\pi/a$ one thus expects $d_{100} = a/2$ (a = lattice constant) and for surfaces vicinal to (111) where $Q_{111} = 2\pi\sqrt{3}/a$ one expects $d_{111} = a/\sqrt{3}$. It strongly supports the staircase model that periodic step structure of just those step heights has actually been observed [15] in LEED diffraction studies of thermally oxidized high index $Si-SiO_2$ interfaces vicinal to (100) and (111), from which the oxide has been removed prior to the LEED studies.

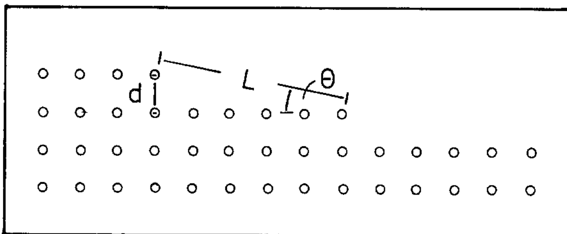

Fig. 3. Sketch of the staircase-like interface structure that can develop on the semiconductor side of a semiconductor-oxide interface prepared on a high index surface. The surface plane is tilted by an angle θ with respect to the high symmetry lattice plane such that periodic steps of height d and period L are formed

At present, based on the studies carried out on high index surfaces of Si, a clear-cut decision whether the valley projection mechanism or the staircase mechanism causes the observed minigaps is not possible. Comparison between the measured size of the minigaps [1, 3, 9, 11, 12] and the ones calculated by the valley projection model [3, 6, 16, 17] or the staircase model [18] does not give conclusive evidence for the one or the other model. This was one of the motives why we decided to search for 1D minigaps in electron inversion layers on high index surfaces of a single-valley isotropic semiconductor such as InSb. Another motivation was given by the fact that the energetically lowest minigaps in electron inversion layers on Si are of inter-valley type [3] and do not have the simple periodical energy structure shown in Fig. 1, that is expected for intra-valley minigaps. Furthermore, these minigaps on Si are rather small, typically $\Delta E \sim 1\,\text{meV} \times n_s[10^{12}\,\text{cm}^{-2}]$, were n_s is the areal electron density in the DES. This does not make them very suitable to study non-linear electrical transport.

We thus decided to search for minigaps in inversion layers on a direct gap semiconductor with a single and isotropic conduction band minimum. InSb was chosen because the realization of high mobility inversion layers in MOS-structures on InSb had previously been demonstrated [19] and the subband structure had been studied extensively on high symmetry surfaces [20–23]. We also expected relatively large minigaps on InSb, since due to the low effective mass of the conduction electrons the energy scale for a given wave vector is much larger on InSb than on Si.

In the following we will first make a few remarks on sample preparation and experimental techniques. We then will present and discuss the results ob-

tained in conductance versus gate voltage studies of electron inversion layers on high index surfaces of InSb in the absence of magnetic fields. Magnetoconductance experiments are discussed in the next chapter. They show that lense and combined orbits can be identified at Fermi energies above the lowest minigap. Our results on InSb are summarized in a concluding chapter.

II. Sample Preparation and Characterization

MOS-samples are prepared on commercially available InSb wafers [24]. The characteristic properties of the substrate material at 77 K are as follows: resistivity $\rho \simeq 2$–$6\,\Omega$cm, carrier concentration 1–5 $\times 10^{14}$ cm^{-3}, and hole mobility 4,000–9,500 cm^2/Vs. From wafers with (111), (110), or (100) surface orientation plateletts of typically 5×6 mm^2 are cut. After the surface normal is checked with Laue diffraction to an accuracy of about $\pm 0.2°$ the samples are transfered to a polishing jig which allows lapping of a high index surface tilted by a well defined angle from the nearest high symmetry plane. After the desired surface is lapped it is polished with alumina powder of decreasing grain size down to 1 µm. This is followed by a chemo-mechanical polish [25] in a low concentration (0.0025 to 0.05 vol. %, depending on surface orientation) bromine in methanol solution [23]. On thus prepared surfaces a typically 300 nm thick layer of SiO_2 is deposited as gate insulator in a plasma-enhanced low pressure CVD process at low substrate temperatures (typically 80 °C) [26]. The fabrication of a MOS capacitor is finished after the deposition of a thin (~ 5 nm) high resistivity ($\sim 1{,}000\,\Omega/\square$) NiCr gate. The surface orientation of the finished samples is again measured by Laue diffraction.

The electronic properties of the MOS samples are characterized at liquid helium temperatures by capacitance-voltage (CV) curves and inversion layer conductance studies. From low frequency CV curves we determine the oxide capacitance per unit area $C_{ox} = \varepsilon_0 \varepsilon_{ox}/d_{ox}$, where ε_{ox} and d_{ox} are the relative dielectric constant and the thickness of the gate oxide, respectively. The CV curves also yield information on the flat band voltage V_{FB}, inversion threshold V_t and the density of charged surface states N_{ss}. A typical CV-curve is shown in Fig. 4. Flatband voltages in our samples are always negative ranging from -12 V to -6 V. Correspondingly we estimate fixed surface states $N_{ss} \sim 2$–8×10^{11} cm^{-2}. Hysteresis in the CV curves shows that the charge state of some surface states can be changed at liquid helium temperatures. These fast states typically have densities of order 1×10^{11} cm^{-2}. At gate voltages V_g above the threshold voltage V_t, which typically ranges from -6 V to 0 V in our samples, an electron inversion layer is formed with inversion carriers of density

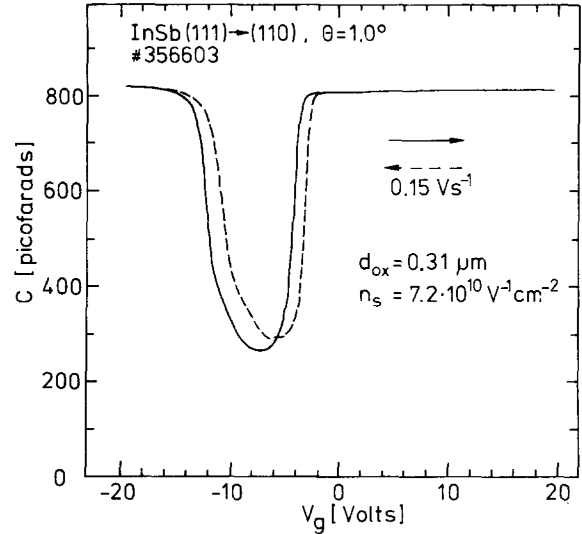

Fig. 4. Capacitance-voltage curves of a InSb MOS-capacitor (gate area 7.2 mm^2) measured at $T = 4.2$ K and low modulation frequency (8 Hz) of the gate voltage Vg. The arrows indicate the direction into which Vg is changed. As indicated in the top of the figure the surface normal of the high index surface is tilted by $\theta = 1°$ from the one of the (111) surface towards the one of the next (110) surface

$$\mathbf{n_{inv} = (C_{ox}/e)(V_g - V_t)}. \tag{3}$$

To characterize the inversion layer properties we measure the inversion channel conductivity at low temperatures and also in high magnetic fields. To avoid the complications connected with the fabrication of n-type ohmic contacts on InSb [19] we use high frequency methods to measure the inversion channel conductivity. One method we use is to measure the gate voltage induced change in microwave transmission or reflection [28, 29]. At microwave frequencies (here about 35 GHz) the gate voltage induced change in the microwave signal is still proportional to the quasi-static conductivity σ of the mobile inversion carriers since one has $\omega\tau \ll 1$, where ω is the microwave frequency and τ the momentum relaxation time of inversion carriers, which typically is $\tau \leqq 10^{-13}$ s. As a second high-frequency method to measure the inversion channel conductivity at low temperatures we use radio frequencies of order 30 MHz and capacitive source-drain contacts [30]. In our experiments we have to measure the channel conductivity in two directions, parallel and perpendicular to the superlattice direction $\vec{G}$. For radio

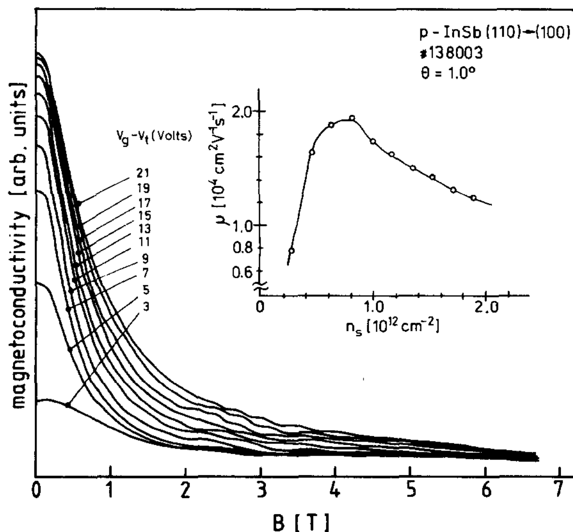

Fig. 5. Magnetoconductivity of inversion electrons in a MOS-capacitor fabricated on a high index surface vicinal to (110) at $T = 4.2$ K. Here the magnetoconductivity is measured by the gate voltage induced change of the transmission of microwaves of frequency 35 GHz. The mobilities displayed in the insert are extracted from the magnetic field value $B_{1/2}$, where the conductivity drops to half its zero field value as discussed in the text

frequency experiments we therefore evaporate three aluminum pads on the resistive NiCr gate in an L-shaped geometry as capacitive source-drain contacts. In the microwave measurements of the inversion conductivity we measure the two directions by rotating the sample by 90° with respect to the direction of the E-field of the microwaves [29].

At microwave frequencies inversion electron density and mobility are extracted from magnetoconductivity experiments as pictured in Fig. 5. The gate voltage induced microwave signal is proportional to $\sigma_{xx}(B)$. At low fields we can approximate $\sigma_{xx}(B)$ by the classical expression

$$\sigma_{\mathbf{xx}}(\mathbf{B}) = \sigma_0/(1+\omega_c^2\tau^2) \quad \text{with} \quad \omega_c\tau = \mathbf{eB}\cdot\tau/\mathbf{m}^*. \qquad (4)$$

From the magnetic field $B_{1/2}$ where $\sigma_{xx}(B_{1/2}) = \sigma_0/2$ we thus can determine an effective mobility $\mu = e\tau/m^* = 1/B_{1/2}$ which is shown in the insert of Fig. 5. Typical peak mobilities in samples prepared on high index surfaces of InSb and measured at 4.2 K range from 1.5 to $4\times10^4\,\text{cm}^2/\text{Vs}$ and are found at inversion electron densities n_s between 0.5 and $1\times10^{12}\,\text{cm}^{-2}$.

At higher magnetic fields the magnetoconductance shows Shubnikov-de Haas (SdH) oscillations [2, 4]. A detailed analysis of the SdH-oscillations, which is discussed elsewhere [21, 23], shows that up to four subbands are occupied in inversion layers on InSb at high densities n_{inv}. Studies of the dependence of the SdH oscillations on surface orientation show that the subband structure on InSb is isotropic as expected [23]. Also the distribution of the total density of mobile inversion electrons $n_s = \sum n_s^i$ among the subbands i ($i = 0, 1, 2 \ldots$), where n_s^i is the occupation of the ith subband as determined from SdH experiments, is found to be independent of surface orientation. Within the accuracy of our experiments (5%) we also find that the total inversion density n_s derived from the SdH experiments agrees with the induced electron density n_{inv} (3), so that in the following we always use $n_{\text{inv}} = n_s$ [23]. In agreement with theory [22] we find that up to densities of $n_s = 3\times10^{12}\,\text{cm}^{-2}$ approximately 65% of the total electron density n_s occupies the lowest subband $i = 0$. The minigap induced conductance structures that are discussed in the following are only observed in this lowest subband. Only in this subband we achieve sufficient high carrier concentration n_s^0 that the Fermi level can be swept across the minigap for the surface orientations studied here.

III. Results and Discussion

A. Conductance Anomalies

A detailed understanding of the subband structure on high symmetry surfaces of InSb is a prerequisite to be able to detect and identify the structure connected with minigaps on high index surfaces. The fact that several subbands are occupied in electron inversion layers on InSb causes structure in the conductance versus gate voltage curves that is isotropic and not connected with minigaps [21–23]. The appearance of minigaps then causes additional structure in the conductance curves that can only be separated from structure caused by occupation of higher subbands through its anisotropic nature [29].

To illustrate this Fig. 6 displays the derivative of the conductance $d\sigma/dV_g$, which is related to the field effect mobility [2], versus gate voltage V_g as observed in two samples with high index surfaces vicinal to (111). These curves are measured for two orientations of the high frequency field E in the surface plane, namely $\vec{E}\parallel\vec{G}$ and $\vec{E}\perp\vec{G}$. For both orientations we observe fine structure in $d\sigma/dV_g$. Most of the structure, however, is essentially isotropic in that it appears for both orientations of $\vec{E}$ at the same V_g and arises from occupation of higher subbands [21, 23]. Only the structure marked by the arrow is strongly anisotropic and observed only with $\vec{E}\parallel\vec{G}$. This structure is identified as being caused by

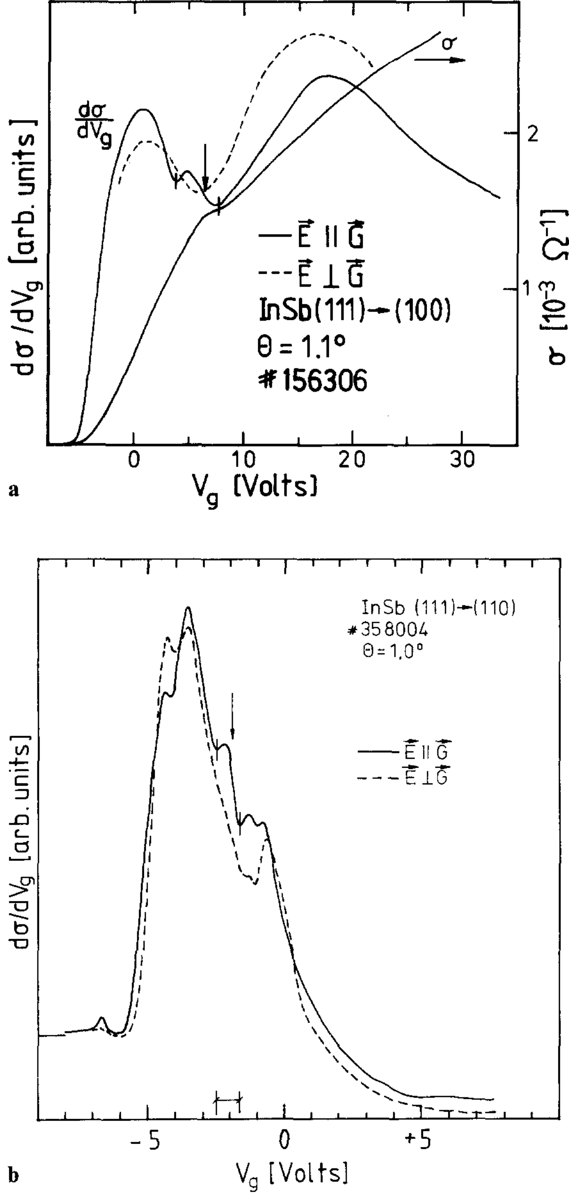

Fig. 6a and b. Derivative of the inversion electron conductivity $d\sigma/Vg$ measured at $T=4.2$ K for two orientations of the high-frequency field $\vec{E}$ in the surface plane, $\vec{E}\parallel\vec{G}$ and $\vec{E}\perp\vec{G}$. The data in (**a**) are measured with microwaves (35 GHz) and also show σ (right scale) for $\vec{E}\parallel\vec{G}$. Here the absolute scale of σ is calculated from the measured values of n_s and μ. The data in (**b**) are measured at radio frequency (30 MHz) using 3 capacitive contacts. The arrow marks the position and the vertical bars the width of the minigap induced structure. From the former we extract the position and from the latter the size of the minigap

a 1D minigap [29], first because of its shape and dependence on the field orientation and, second, because of the electron density at which it occurs.

The effect of a 1D minigap in the 2D subband structure on the inversion channel conductance has first been experimentally observed by Cole et al. [1] for both source-drain field directions $\vec{E}\parallel\vec{G}$ and $\vec{E}\perp\vec{G}$. Ando has theoretically investigated the conductivities $\sigma_{xx}(\vec{E}\parallel\vec{G})$ and $\sigma_{yy}(\vec{E}\perp\vec{G})$ for both, zero and finite magnetic field [8, 31] and found that for $B=0$ there is a pronounced maximum in σ_{xx} but only a weak structure in σ_{yy}, in qualitative agreement with experimental results on Si [1] and those presented here. The anisotropic structure in Fig. 6 corresponds to a relative maximum of σ_{xx} and is not observed for σ_{yy}. The identification of this structure as being caused by a 1D minigap is further confirmed by its position on the gate voltage scale as indicated by the arrows. Using (3) we can convert the gate voltage into an n_s-scale and, assuming that the occurrence of minigaps does not significantly change the relative occupation of the ground subband n_s^0/n_s, into a density n_s^0, where the minigap is centered. This value then can be compared with the value predicted from both, the valley projection and the staircase model. In these models the center of the minigap in a conductance vs gate voltage curve is expected when the electron density n_s^0 in the ground subband is such that the Fermi energy lies in the center of the lowest minigap in this subband. For InSb with spin-degeneracy $g_s=2$ and no valley-degeneracy this is the case when

$$\mathbf{n}_s^0=\mathbf{g}_s(\mathbf{G}/2)^2/(4\pi)=(\mathbf{Q}^2/8\pi)\cdot\sin^2\theta \tag{5}$$

In Fig. 7 we compare the experimentally derived values of n_s^0 where we observe anisotropic structure in the conductance vs gate voltage curves for samples with surfaces vicinal to (111) (Fig. 7a) and to (110) (Fig. 7b) with those calculated by (5). Note that for (111) we have $Q_{111}=2\pi\sqrt{3}/a$ and for (110) $Q_{110}=3\pi\sqrt{2}/a$ with $a=6.48$ Å for InSb. For all samples the agreement between experiment and theoretical prediction is within experimental error. From this we conclude that both models correctly predict the observed position of minigaps. For the staircase model the here observed positions are caused by step heights which are also the most likely ones [18]. Thus we cannot differentiate between the valley projection model and the staircase model from the observed density n_s^0 at which the minigaps are located.

From the widths Δn_s of the anisotropic structure of the conductance curves (marked in Fig. 6) one can also infer on the size of the observed 1D minigaps. If one approximates the density of states in the vicinity of the minigap [31] by the 2D density of states $D(E)=m^*/(\pi\hbar^2)$ and takes into account the dependence of the effective mass m^* in subbands on

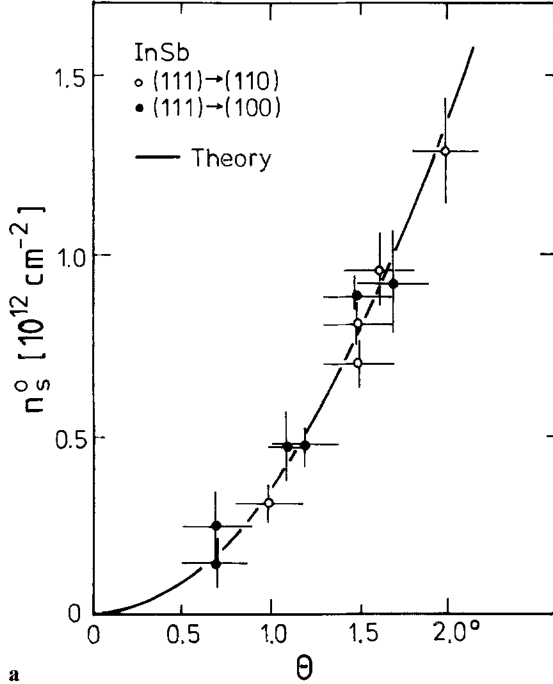

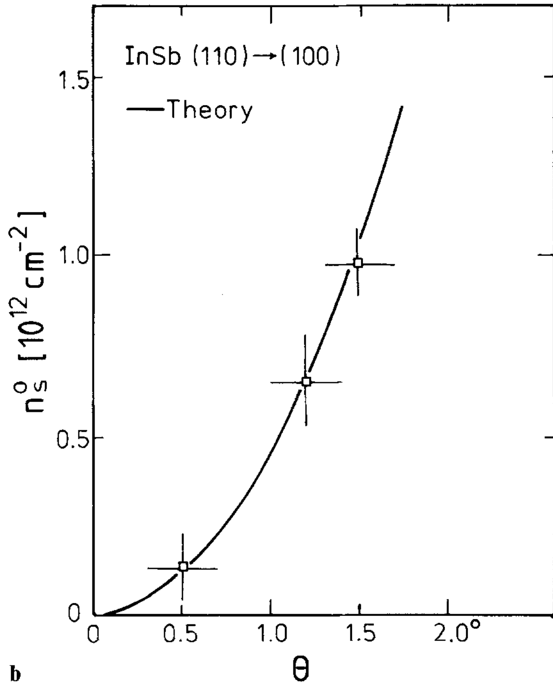

Fig. 7a and b. Angular dependence of the electron density n_s^0 in the ground subband at which the Fermi level lies in the center of the lowest minigap for surfaces (**a**) vicinal to (111) and (**b**) vicinal to (110)

InSb on energy [20, 23] one may approximately convert the width of the structure in σ_{xx} into a size of the minigap according to:

$$\Delta \mathbf{E} = \Delta \mathbf{n}_s^0 \cdot \pi \hbar^2 / \mathbf{m}^*. \qquad (6)$$

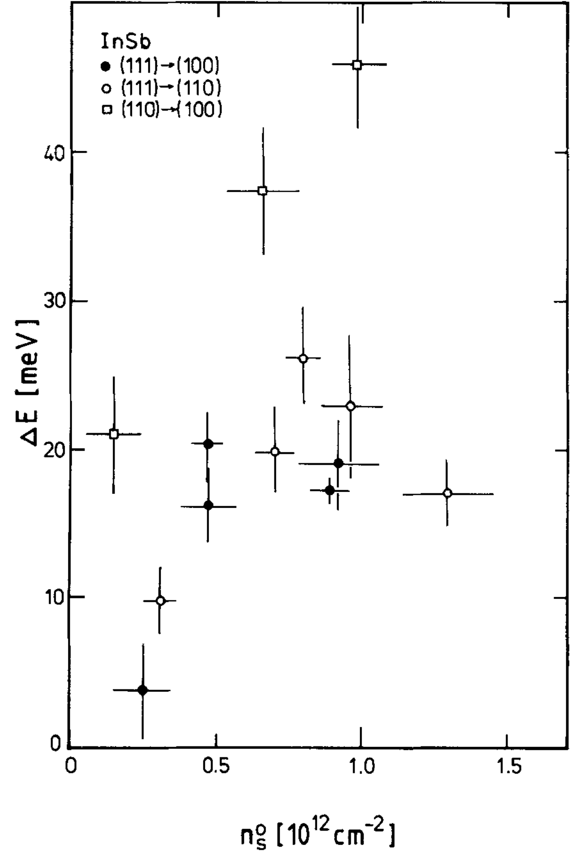

Fig. 8. Size of the lowest minigap ΔE vs. electron density n_s^0 in the ground subband at which it is observed in the conductance voltage curves (see Fig. 6) for samples with surfaces vicinal to (111) and (110)

The thus determined size of the minigaps is displayed in Fig. 8 versus the electron density n_s^0 at which the minigap is observed. At low densities n_s^0 the size of the minigap rises approximately in proportion to n_s^0, similarly as found on high index surfaces of Si [3, 11, 12]. On surfaces vicinal to (111) it appears to be essentially independent on the tilt direction of the surface normal. The minigaps observed on surfaces vicinal to (110) seem to be nearly twice as high as on surfaces vicinal to (111). However, there have only been 3 samples vicinal to (110) on which we have observed minigap induced structure in σ so that we cannot be sure whether this difference is significant. We wish to point out, that sizes of minigaps observed on InSb, which have typical values of $\Delta E = 20$ meV at $n_s^0 = 10^{12}$ cm^{-2}, are nearly twenty times higher than those observed in electron inversion layers on high index surfaces of Si at the same electron density. In this comparison one has to keep in mind that the minigaps on InSb are

caused by interaction of identical valleys in adjacent Brillouin-zones (intra-valley gaps) whereas those studied most extensively on Si [1, 3, 11, 12] are caused by interaction of different valleys in adjacent Brillouin-zones (inter-valley gaps).

It should be noted that the data shown in Fig. 6 and evaluated in Figs. 7 and 8 are by no means typical. Only a small portion ($\sim 10\%$) of the many samples (~ 200) that we have prepared on high index surfaces and investigated with conductance experiments at low temperatures have shown anisotropic structure in the conductivity. In the majority of samples we have not been able to unambiguously observe anisotropic structure in the conductance vs gate voltage curves, though the inversion channel mobility in these samples has been comparable to the one of those where we have detected minigaps. From this we conclude that sufficiently high mobility is not the only condition that needs to be established to observe minigaps. On surfaces vicinal to Si(100) we have not been able to prepare MOS-capacitors that show minigap induced conductance structure though we have been able to fabricate samples on those surfaces with peak mobilities of $30{,}000\ cm^2/Vs$, comparable to good samples on surfaces vicinal to (110) or (111). A characteristic feature of the samples on surfaces vicinal to (100) is that the SdH oscillations of the magnetoconductivity are significantly more damped than on other surfaces studied. This indicates that surfaces vicinal to (100) have a higher inhomogeneity than other surfaces. Such an inhomogeneity could explain both the damping of the SdH-oscillations and the damping of minigap induced conductance structure.

We also want to point out that the magnitude of the minigap induced conductance structure on InSb is much weaker than on Si. This is surprising if one notes that on InSb the relative size of the minigaps at a typical density $n_s^0 = 10^{12}\ cm^{-2}$ is with $\Delta E/E \simeq 0.2$ about the same as on Si, whereas the absolute value of ΔE is much larger as on Si. One possible cause of the much weaker structure on InSb could be the fact that there are states from higher subbands ($i = 1, 2, \ldots$) that are energetically degenerated with the minigaps in the ground subband. Such states would decrease singularities in the density of states around the minigap and hence decrease the conductance anomalies. We think it more likely that surface inhomogeneities at the $InSb-SiO_2$ interface dampen the minigap induced structure. Whereas the $Si-SiO_2$ interface is known to be perfect within one lattice constant [32], little is known about the interface between InSb and SiO_2 in our MOS-structures. Since we are able to reproducibly fabricate MOS-samples on high index surfaces with peak mobilities of typically $20{,}000\ cm^2/Vs$, the surface inhomogeneity that is discussed here must have relatively little effect on mobility but strong effect on the minigap structure. The mobility tests perturbations which are similar in length as the extension of the inversion subband wavefunction, which is ~ 100 Å for the lowest subband on InSb [22]. Insofar an inhomogeneity that destroys minigap structure but has little effect on mobility must have a much smaller scale. The staircase model could explain our observations qualitatively. Surface steps of heights $d < a$ can easily be imagined to critically depend on sample preparation and vary laterally across the sample thus creating an inhomogeneous interface potential. Since such steps are still very small in comparison to the extension of the inversion electron wavefunction they might have little effect on mobility. On Si where the $Si-SiO_2$ interface is formed by a high temperature thermal oxidation one probably has very similar interface properties in samples of comparable mobility. Insofar a staircase model also might explain why minigaps on high index surfaces of Si are observed on all high mobility samples, whereas this is not true on InSb.

In our studies on InSb we have also tried to observe the minigaps optically by looking for anisotropic structure in the infrared absorption, caused by transitions across the minigap. Such interminiband absorption is relatively easily detected on high index surfaces of Si [3, 11, 12]. We have tried similar experiments on InSb with both, infrared spectroscopy at fixed laser frequencies [11, 12] and frequency-swept experiments using a Fourier-transform spectrometer [3]. In none of those experiments were we able to observe minigap induced structure in the infrared absorption though, judged by the relative and absolute size of the minigap, we should expect structure that is easily observable. The only explanation that we can offer is again surface inhomogeneity. If only 20% of the sample surface shows minigap structure it would be difficult to detect this optically, where one essentially adds the contributions from different parts of the sample. In a transport experiment where one has both series and parallel contributions from different areas of the sample one, however, probably could still observe minigap induced structure. All the above discussed features of our conductance studies make it very likely that inhomogeneities at the $InSb-SiO_2$ interface play an essential role in the observability of minigap induced structure. Such inhomogeneities can easily be imagined in the staircase interface model proposed by Volkov et al. [14].

B. Magnetoconductance Effects

The appearance of minigaps in the 2D subband structure also has strong effects on the SdH-oscillations [1, 31, 33]. In weak magnetic fields applied perpendicular to the 2DES the electrons are forced to move on constant energy contours as pictured in Fig. 1. For a Fermi energy below the lowest minigap the orbits of electrons at E_F are essentially circles. If E_F lies just above the first minigap one has lense shaped orbits and open orbits (see Fig. 1). This change in the geometry of the orbit as the Fermi energy sweeps across the minigap also has a strong effect on the SdH oscillation spectra. Since the frequencies of the SdH oscillations in a sweep of n_s or of $1/B$ are proportional to the area enclosed by the orbit, they are strongly affected by the orbit geometry. Further complexity in the SdH spectra occurs at increased magnetic field strengths which cause magnetic field induced tunneling through the minigap [1, 33], so-called magnetic breakdown [34].

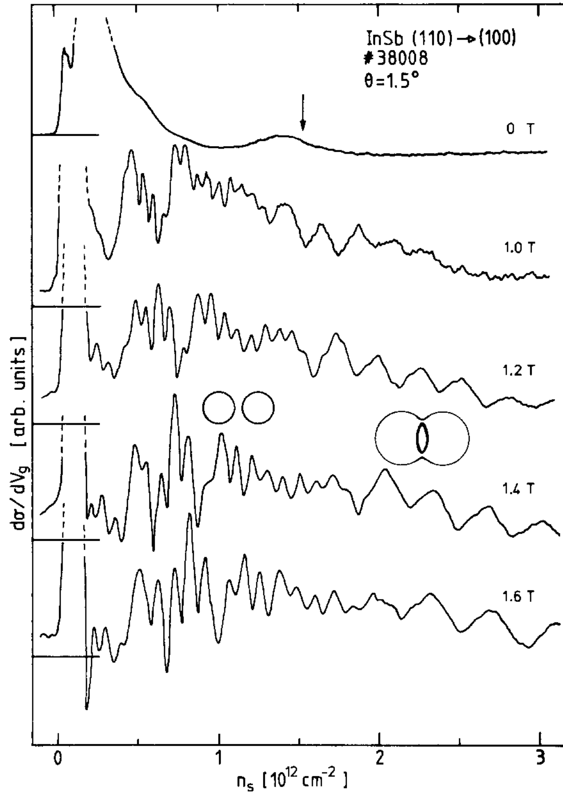

Fig. 9. Shubnikov-de Haas oscillations of the conductance derivative $d\sigma/dVg$ versus inversion electron density n_s at various magnetic field values B. The data are measured with the radio frequency method at $T=4.2$ K and $\vec{E}\parallel\vec{G}$ on a sample fabricated on a high index surface vicinal to (110). The structure at $B=0$ and $n_s \simeq 1.3\times10^{12}$ cm^{-2} is caused by the minigap. At finite magnetic fields one sees with n_s below the minigap rapid SdH-oscillations that arise from circle orbits in the ground subband, and with n_s above the minigap lower frequency SdH-oscillations caused by lense shaped orbits as indicated

On a high mobility InSb sample with its surface orientation vicinal to (110), which shows a strong minigap induced conductance anomaly at $B=0$, we have studied the SdH spectra in detail. Figure 9 shows a sequence of SdH spectra measured in $d\sigma/dVg$ in a sweep of n_s. In the low magnetic field curves (e.g., $B=1$ T) one notices a sudden increase of the SdH period as the Fermi energy is moved accross the minigap. With E_F below the minigap (in Fig. 9 at $n_s<1.3\times10^{12}$ cm^{-2}) the dominant SdH frequency reflects the circular electron orbit in the ground subband. The decrease of the SdH frequency as E_F increases above the minigap thus results from an orbit with significantly smaller area, which we interpret as the lense shaped orbit also shown in Fig. 1.

A more detailed analysis of the SdH frequencies that are contained in the spectra of Fig. 9 becomes possible by Fourier transform of the spectra [33] as displayed in Fig. 10. At the lower field values one notices two SdH frequencies below the one of the circular orbit in the ground subband. The strength of the lowest one decreases rapidly with increasing B whereas the strength of the next higher one is little affected by magnetic field. This as well as the relative values of the SdH frequencies leads us to conclude that the lowest SdH frequency is caused by the lense orbit whereas the next higher one reflects the circular orbit in the $i=1$ subband, that is already occupied at rather low densities [21, 22]. At the higher magnetic fields additional peaks appear in the Fourier transform spectra above the frequency of the circular orbit in the ground subband. These frequency components of the SdH spectra must be caused by orbits that are larger in area as the circular orbit. These orbits are identified by their frequency as combination orbits, such as a peanut or a lense and circle combination. Such combinations become possible at the higher magnetic fields because of magnetic breakdown across the minigap [33, 34]. The appearance of these orbits as well as the increasing strength of the circular orbit ($i=0$) with increasing magnetic field correlate with the disappearance of the lense orbit as expected by magnetic breakdown. At the highest magnetic fields in Fig. 10 there occurs an additional peak in the Fourier transform spectra at a frequency between the circular orbits of the $i=1$ and $i=0$ subbands. Since this orbit frequency cannot be associated with an expected orbit we have been unable to identify it. Figure 11

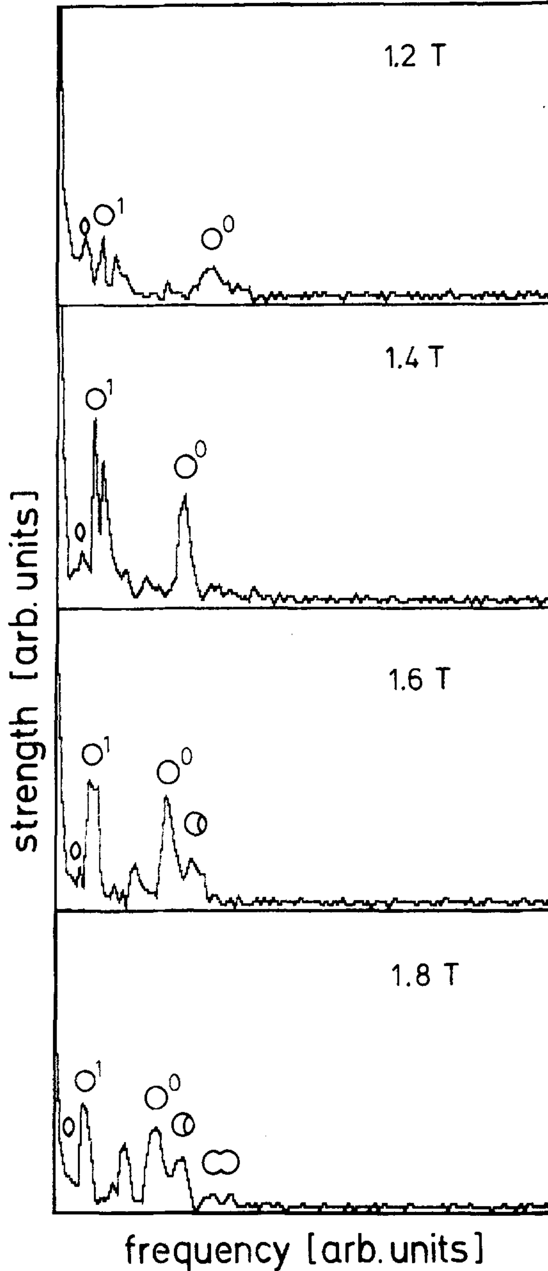

Fig. 10. Fourier spectrum of the SdH-oscillations shown in Fig. 9. Where possible the peaks in the Fourier spectrum are marked by the orbits from which they arise. Circle orbits are not only seen in the ground subband 0 but also in the higher subband 1

shows the magnetic field dependence of the SdH frequencies. As expected they are proportional to $1/B$. Comparing the different frequencies at a given field B one finds that the frequencies of the combination orbits are as expected from the frequencies of the circular and the lense orbit in the ground subband.

The observation of magnetic breakdown in the

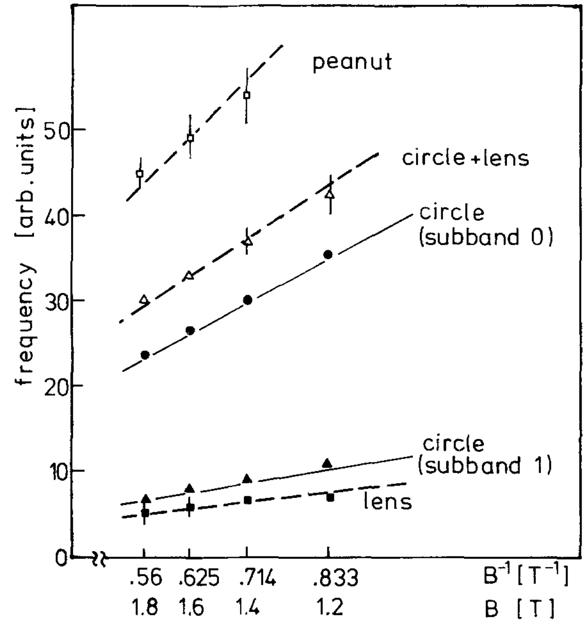

Fig. 11. Magnetic field dependence of the dominant frequencies in the Fourier spectrum in Fig. 10. The orbits that correspond to these frequencies are indicated. The lines through the data all extrapolate to zero frequency at $B^{-1}=0$ as expected

SdH spectra allows us to estimate the minigap in a way quite different from the determination via the $B=0$ conductance anomaly (Eq. (6)). From the magnetic field value B_0 at which breakdown occurs (here $B_0 \simeq 1.2\,\mathrm{T}$) one can estimate ΔE as [33, 34]:

$$\Delta \mathbf{E} \simeq (\mathbf{E_F} \hbar \mathbf{e} \mathbf{B_0}/\mathbf{m}^*)^{1/2} = (\mathbf{E_F} \hbar \omega_c)^{1/2}. \tag{7}$$

For the sample studied in Figs. 9–11 we find $n_s^0 = 0.9 \times 10^{12}\,\mathrm{cm}^{-2}$ and from (7) $\Delta E \simeq 23\,\mathrm{meV}$. This is somewhat lower than the value estimated from the conductance anomaly at $B=0$ via (6), which is $\Delta E \simeq 45\,\mathrm{meV}$. In view of the fact that both ways of determining ΔE are only rather approximate the agreement between the two independently determined values can be considered satisfactory. The magnetoconductance studies discussed above require samples of very good homogeneity and mobility. In most of the samples in which we were able to observe anisotropic conductance anomalies at $B=0$, we were not able to see details of the SdH spectra that are shown above.

IV. Summary and Conclusion

In MOS structures prepared on high index surfaces of InSb we have systematically investigated 1D mi-

nigaps in the single valley subband structure of the two-dimensional electron system created at the semiconductor-oxide interface by field effect. The presence of minigaps is observed in many samples via anisotropic structure in the conductance versus gate voltage curves at liquid helium temperatures. On all those samples with surfaces tilted by a small angle θ ($\leqq 2°$) with respect to a high symmetry (111) or (110) surface the position of the minigap in a sweep of electron density or, equivalently, Fermi energy is found to agree with the predictions of the valley projection model by Sham et al. [3], applied here to the simple case of a single valley semiconductor. However, the energetical positions of the minigaps are equally well explained by the staircase interface model proposed by Volkov et al. [13].

The size of the observed minigap on InSb is found to be relatively large, typically $\Delta E/E_0 \sim 0.2$, where the center energy of the minigap E_0 varies between about 10 meV and 100 meV. Nevertheless we observe that the conductance structure caused by the minigap is comparatively weak. This is attributed to a microscopic structure of the $InSb-SiO_2$ interface that is much more inhomogeneous than the $Si-SiO_2$ interface. Such interface inhomogeneity could also explain why only a relatively small portion of the very many samples investigated showed minigap induced conductance structure though in all samples the inversion electrons had peak mobilities in excess of 10,000 cm^2/Vs at 4.2 K. In the staircase interface model it is relatively easy to imagine how such inhomogeneous interface structure can arise. A clear differentiation as to which of the two discussed models more closely describes reality, however, is not possible by our experiments.

We have also demonstrated that minigaps can be detected in the Shubnikov-de Haas oscillations of the magnetoconductivity of inversion electrons on InSb. The various orbits that become possible by the occurrence of a 1D minigap and magnetic breakdown across such minigaps are clearly detected by the corresponding SdH periods. The magnetic breakdown experiments also allow an independent measurement of the size of the minigap which is found to reasonably agree with the one derived from the conductance structure in the absence of magnetic fields.

Our studies also show that in spite of the relatively large size of the minigaps observed here ($\Delta E \geqq 20$ meV) MOS-structures on InSb are not an ideal system to investigate 1D minigaps in a two-dimensional electron system and their effect on electrical transport. In this system the problem of interface inhomogeneity caused by irreproducible preparatory conditions seems unsolvable. Since our studies show conclusively that large 1D minigaps can be observed in the 2D subband structure derived from a single conduction band minimum the question arises whether there exist similar systems with more reproducible interfaces. We believe that heterostructures prepared by molecular beam epitaxy on high index surfaces of III–V compounds, such as GaAs, are very promising systems. In such systems one might be able to combine the simplicity of the minigap structure derived from a single valley conduction band found here with excellent interface conditions that can be reproducibly prepared by molecular beam epitaxy [see e.g. 35, 36] with qualities comparable to or better than the $Si-SiO_2$ interface. Such heterostructures then might allow a clear differentiation of the above discussed models as well as a whole spectrum of novel experiments on non-linear electrical transport accross minigaps.

We want to thank M. Horst, U. Merkt, and L.J. Sham for stimulating discussions. The financial support of the Deutsche Forschungsgemeinschaft is gratefully acknowledged.

References

1. Cole, T., Lakhani, A.A., Stiles, P.J.: Phys. Rev. Lett. **38**, 722 (1977)
2. For an extensive review on two-dimensional electron systems see: Ando, T., Fowler, A.B., Stern, F.: Rev. Mod. Phys. **54**, 437 (1982)
3. Sham, L.J., Allen, S.J., Jr., Kamgar, A., Tsui, D.C.: Phys. Rev. Lett. **40**, 472 (1978)
4. Fowler, A.B., Fang, F.F., Howard, W.E., Stiles, P.J.: Phys. Rev. Lett. **16**, 901 (1966)
5. Ohkawa, F.J., Uemura, Y.: J. Phys. Soc. Jpn. **43**, 907 (1977)
6. Sham, L.J., Nakayama, M.: Phys. Rev. B**20**, 734 (1979)
7. Ando, T.: Phys. Rev. B**19**, 3089 (1979)
8. Ando, T.: Surf. Sci. **98**, 327 (1980)
9. Tsui, D.C., Sturge, M.D., Kamgar, A., Allen, S.J., Jr.: Phys. Rev. Lett. **40**, 1667 (1978)
10. Kvon, Z.D., Kol'tsov, B.B., Neizvestnyi, I.G., Ovsyuk, V.N.: JETP Lett. **33**, 571 (1981)
11. Sesselmann, W., Kotthaus, J.P.: Solid State Commun. **31**, 193 (1979)
12. Kamgar, A., Sturge, M.D., Tsui, D.C.: Phys. Rev. B**22**, 841 (1980)
13. Volkov, V.A., Sandomirskii, V.B.: JETP Lett. **27**, 651 (1978)
14. Volkov, V.A., Petrov, V.A., Sandomirskii, V.B.: Sov. Phys. Usp. **23**, 375 (1980)
15. Ol'shanetskii, B.Z., Rzhanov, A.V.: JETP Lett. **32**, 313 (1980)
16. Nakayama, M., Sham, L.J.: Solid State Commun.: **28**, 393 (1978)
17. Ohkawa, F.J.: J. Phys. Soc. Jpn. **46**, 855 (1979); Surf. Sci. **98**, 350 (1980)
18. Ohkawa, F.J.: Phys. Rev. B**24**, 7297 (1981)
19. Kotera, N., Katayama, Y., Komatsubara, K.F.: Phys. Rev. B**5**, 3065 (1972)

20. Därr, A., Kotthaus, J.P., Koch, J.F.: Solid State Commun. **17**, 455 (1975)
21. Därr, A., Kotthaus, J.P.: Surf. Sci. **73**, 549 (1978); Därr, A.: Dissertation, TU München 1981 (unpublished)
22. Takada, Y., Arai, K., Uchimura, N., Uemura, Y.: J. Phys. Soc. Jpn. **49**, 1851 (1980)
23. Merkt, U., Horst, M., Evelbauer, T., Kotthaus, J.P.: (to be published)
24. InSb substrates were fabricated by M.C.P. Electronics, Ltd. Alperton, England
25. Sullivan, M.V., Kolb, G.A.: J. Electrochem. Soc. **110**, 585 (1963)
26. Mackens, U., Merkt, U.: Thin Solid Films **97**, 53 (1982)
27. See e.g. Sze, S.M.: Physics of semiconductor devices. 2nd Edn. New York: Wiley & Sons 1981
28. Koch, J.F.: Festkörperprobleme. (Advances in Solid State Physics). Queisser, H.J. (ed.), Vol. XV, pp. 79–112. Braunschweig: Pergamon-Vieweg 1975
29. Evelbauer, T., Merkt, U., Kotthaus, J.P.: Physica **117**B & **118**B, 670 (1983)
30. Dolgopolov, V., Mazuré, C., Zrenner, A., Koch, F.: J. Appl. Phys. **55**, 4280 (1984)
31. Ando, T.: J. Phys. Soc. Jpn. **47**, 1595 (1979)
32. see e.g. Krivanek, O.L., Tsui, D.C., Sheng, T.T., Kamgar, A.: The physics of SiO_2 and its interfaces. Pantelides, S.T. (ed.), pp. 356–361, New York: Pergamon 1978
33. Matheson, T.G., Higgins, R.J.: Phys. Rev. B**25**, 2633 (1982)
34. Pippard, A.B.: Proc. R. Soc. (London) A**270**, 1 (1962)
35. Ploog, K.: Annu. Rev. Mater. Sci. **11**, 171 (1981)
36. Weimann, G., Schlapp, W.: Appl. Phys. Lett. **46**, 411 (1985)

T. Evelbauer
VALVO RHW
der Philips GmbH
Stresemannallee 101
D-2000 Hamburg 54
Federal Republic of Germany

A. Wixforth
J.P. Kotthaus
Institut für Angewandte Physik
Universität Hamburg
Jungiusstrasse 11
D-2000 Hamburg 36
Federal Republic of Germany